Journal of the Ceramic Society of Japan 133 [9] 562-568 2025
DOI https://doi.org/10.2109/jcersj2.25049

JCS-Japan

FULL PAPER

Atmospheric pressure hydrothermal synthesis and characterization of hollandite-type α-$Mn_{1-x}Ti_xO_2$ for rechargeable magnesium battery cathodes

Masanao Ishijima[1,†], Yu Sakano[1], Kentaro Okada[1], Tamao Ishida[2], Kiyoshi Kanamura[1], Toshihiko Mandai[3] and Koichi Kajihara[1,‡]

[1] Department of Applied Chemistry for Environment, Graduate School of Urban Environmental Sciences, Tokyo Metropolitan University, 1–1 Minami-Osawa, Hachioji, Tokyo 192–0397, Japan
[2] Research Center for Artificial Photosynthesis (ReCAP), Osaka Metropolitan University, 3–3–138 Sugimoto, Sumiyoshi-ku, Osaka 558–8585, Japan
[3] Research Center for Energy and Environmental Materials (GREEN), National Institute for Materials Science (NIMS), 1–1 Namiki, Tsukuba, Ibaraki 305–0044, Japan

Hollandite-type α-MnO_2 and its solid solutions with TiO_2 for the cathode active materials of rechargeable magnesium batteries were synthesized with a hydrothermal method under atmospheric pressure through the oxidation of Mn^{2+} ions with ammonium persulfate [$(NH_4)_2S_2O_8$] within 2 h. The solubility limit of Ti in α-$Mn_{1-x}Ti_xO_2$ was $x \simeq 0.2$, and average particle size decreased with an increase in x. Despite the high surface area, α-$Mn_{1-x}Ti_xO_2$ exhibited lower catalytic activity for oxidative electrolyte decomposition and better discharge capacity retention than α-MnO_2. Capacity retention was the highest and the increment of charge overpotential during cycles was the smallest at $x = 0.2$.

Key-words : Hollandite-type α-$Mn_{1-x}Ti_xO_2$, Atmospheric pressure hydrothermal synthesis, Rechargeable magnesium battery

[Received April 1, 2025; Accepted June 9, 2025]

1. Introduction

Rechargeable magnesium batteries (RMBs) with magnesium metal anodes have attracted attention as next generation batteries because of the abundance of magnesium, high safety, and high theoretical capacity. Potential candidates for high-voltage cathode active materials of RMBs include transition metal spinel oxides,[1–6] hollandite-type α-MnO_2,[7–11] and amorphous oxide derived by the delithiation of $Li_2Ti_{1/3}Mo_{2/3}O_3$.[12] A crucial issue for the cathode materials of RMBs is to facilitate the migration of Mg^{2+} ions while mitigating their strong Coulombic interactions with anion sublattice. From this viewpoint, α-MnO_2 is attractive because its one-dimensional channels along the c axis are large enough to accommodate Mg^{2+} ions. The theoretical discharge capacity of α-MnO_2 is 308 mA h g^{-1}.[13] However, the insertion of Mg^{2+} ions up to 280 mA h g^{-1} leads to the destruction of the crystal structure of α-MnO_2.[14] In addition, the high catalytic activity of Mn induces oxidative electrolyte decomposition during charging and disturbs the extraction of Mg^{2+} ions. To overcome these problems, the partial cation substitutions of the crystalline lattice of α-MnO_2 have been investigated. For example, V doping into α-K_xMnO_2 enhanced the stability of the α-K_xMnO_2 phase and increased capacity retention upon cycling.[15] Recent experimental evidence has also indicated that the co-insertion of alkali ions mitigates the distortion of channels in α-MnO_2 associated with the insertion of Mg^{2+} ions, leading to a decrease in discharge overpotential and an increase in discharge capacity.[16] Another candidate for the cation substitution of α-MnO_2 include Ti, because TiO_2 has a polymorph with hollandite structure,[17,18] and it may facilitate the formation of hollandite-type α-$Mn_{1-x}Ti_xO_2$ solid solutions.

The conventional way of synthesizing hollandite-type α-MnO_2 is the hydrothermal oxidation of Mn^{2+} ions with persulfate ($S_2O_8^{2-}$) ions under the presence of structural template cations such as K^+ and NH_4^+ ions. Typical reaction temperatures are ~120–180 °C[15,19–26] and pressure vessels are routinely used. However, α-MnO_2 has been prepared by oxidizing Mn^{2+} ions with O_2 in aqueous sulfuric acid solutions at 25 °C,[27] treating Mn_2O_3 in aqueous sulfuric acid solutions at 95–100 °C,[28] oxidizing Mn^{2+} ions with MnO_4^- ions in water at 100 °C,[29] and reducing MnO_4^- ions in ethanol at 78 °C,[30] indicating that α-MnO_2

† Corresponding author: M. Ishijima; E-mail: ishijima@tmu.ac.jp
‡ Corresponding author: K. Kajihara; E-mail: kkaji@tmu.ac.jp

can be formed as the primary phase bellow 100 °C. In addition, the decomposition temperature of $S_2O_8^{2-}$ ions is also lower than 100 °C (~85–90 °C).[31] Indeed, the synthesis of α-MnO_2 through the oxidation of Mn^{2+} ions with ammonium persulfate [$(NH_4)_2S_2O_8$] or potassium persulfate ($K_2S_2O_8$) in a boiled water was reported, whereas the precursor solution was acidified with H_2SO_4 and other additives were not used.[32] These considerations prompted us to develop an easy way to hydrothermally synthesize α-MnO_2 at ~100 °C under atmospheric pressure through the oxidation of Mn^{2+} ions with $S_2O_8^{2-}$ ions. Synthesis under atmospheric pressure in conventional glass containers offers a practical way for scalable synthesis, and the ease of stirring is suitable for the improvement of uniformity of samples.

In this paper, we developed a facile and rapid atmospheric pressure hydrothermal process to synthesize hollandite-type α-MnO_2 for the cathode active materials of RMBs, and examined the partial substitution of Ti into the crystalline lattice of α-MnO_2.

2. Experimental procedure

2.1 Synthesis

Manganese sulfate pentahydrate ($MnSO_4 \cdot 5H_2O$, Fujifilm Wako Pure Chemical), titanyl sulfate ($TiOSO_4 \cdot nH_2O$, Kishida Chemical), ammonium sulfate [$(NH_4)_2SO_4$, Fujifilm Wako Pure Chemical], and $(NH_4)_2S_2O_8$ (Fujifilm Wako Pure Chemical) were dissolved in distilled water in a $MnSO_4$:$TiOSO_4$:$(NH_4)_2SO_4$:$(NH_4)_2S_2O_8$ molar ratio of $1-x$:x:y:1:100 with the total metal (Mn + Ti) content of 15 mmol in a glass screw cap vial of 50 mL capacity. $(NH_4)_2SO_4$ was added to promote the formation of the hollandite-type phases.[21,22] The vial was sealed without being too tight and placed in an aluminum heating block on a hot stirring plate, and the solution was heated to 100 °C and then maintained for t h while stirring. **Caution: The temperature of reaction mixture should not be higher than 100 °C to avoid the explosion of glass vials.** The temperature of the reaction mixture was monitored by inserting a conventional stainless-sheathed K-type thermocouple though the vial cap in several runs, and was used to calibrate the temperature setting of the hot stirring plate. The resulting solid precipitates were centrifuged, washed with water, dried, and heat treated at 300 °C for 5 h in a tube furnace in air.

2.2 Characterization

The resulting powder samples were evaluated by powder X-ray diffraction (XRD, RINT-TTR III, Rigaku), Fourier-transform infrared (FT-IR) spectroscopy (FT/IR-4600, JASCO) using an attenuated total reflection (ATR) unit with a diamond prism, scanning electron microscopy with energy dispersive X-ray spectroscopy (SEM-EDS, JSM-IT800, JEOL and PhenomPro, Thermo Fisher Scientific). Nitrogen adsorption–desorption isomers were recorded using an automatic adsorption instrument (BELSORP MAX, MicrotracBEL) and specific surface area was determined by the Brunauer–Emmett–Teller (BET) method.

2.3 Electrochemical analysis

Dry composite cathodes were prepared by mixing the powder sample, acetylene black (AB, Denka; electrically conductive support), and poly(tetrafluoroethylene) (PTFE, Du Pont-Mitsui Fluorochemicals; binder) in a mass ratio of 60:30:10, and pressing ~2 mg of the composite onto an Al mesh. Electrochemical measurements of the composite cathodes were conducted in an Ar-filled glovebox with a three-electrode cell using a Mg ribbon (99.9 %, Yoneyama Yakuhin Kogyo) as the counter electrode, and a Ag wire immersed in a triglyme (G3, Kanto Chemical) solution of 0.01 mol dm^{-3} $AgNO_3$ (Kanto Chemical) and 0.1 mol dm^{-3} magnesium bis(trifluoromethanesulfonyl) amide ($Mg[TFSA]_2$, Kishida Chemical) as the reference electrode. Two types of electrolytes, i.e., 0.3 mol dm^{-3} [Mg(G4)][TFSA]$_2$/[C_3mPyr][TFSA],[33,34] prepared from tetraglyme (G4, Kishida Chemical), $Mg[TFSA]_2$, and 1-methyl-1-propylpyrrolidinium bis(trifluoromethanesulfonyl)amide ([C_3mPyr][TFSA], Kanto Chemical), and 0.3 mol dm^{-3} G3 solution of magnesium tetrakis(hexafloroisopropyloxy)borate ($Mg[B(HFIP)_4]_2$),[35–37] were used. The water contents of these electrolytes measured using a Karl Fischer titrator (MKC-710, Kyoto Electronics Manufacturing) were ~45–65 ppm. Cyclic voltammetry was performed at a scan rate of 0.1 mV s^{-1} in the potential range from −1.6 to 1.2 V vs. Ag/Ag$^+$ (from 1.0 to 3.8 V vs. Mg/Mg^{2+}). Galvanostatic charge–discharge tests were carried out using an electrochemical analyzer (HZ-Pro and HJ1020mSD8, Hokuto Denko) at 10 mA g^{-1} in the potential range from −1.6 to 0.9 V vs. Ag/Ag$^+$ (from 1.0 to 3.5 V vs. Mg/Mg^{2+}). They were initiated from the discharge step, and the charge capacity was restricted to 154 mA h g^{-1} (half of the theoretical discharge capacity of α-MnO_2). The current densities of cyclic voltammetry and charge–discharge measurements were normalized to the masses of cathode active materials.

3. Results and discussion

Figure 1 shows photographs of a precursor solution prepared at (x, y) = (0, 2) and suspension obtained after heat treatment at 100 °C for 2 h (t = 2). It took ~20 min to heat up to 100 °C, during which the precursor solution started to lose transparency, whereas the suspension was

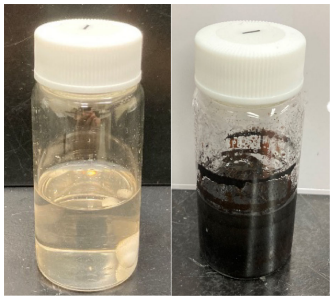

Fig. 1. Photograph of a precursor solution prepared at (x, y) = (0, 2) (left) and suspension obtained by the heat treatment of the precursor solution at 100 °C for 2 h (t = 2) (right).

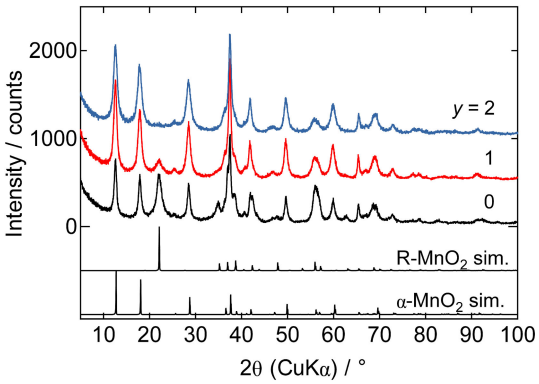

Fig. 2. Powder XRD patterns of the samples prepared at $x = 0$ and $t = 2$ before heat treatment at 300 °C, and simulated pattern of α-MnO_2 and R-MnO_2 calculated using RIETAN-FP[40] and the respective structure parameters reported in Refs. 38) and 39).

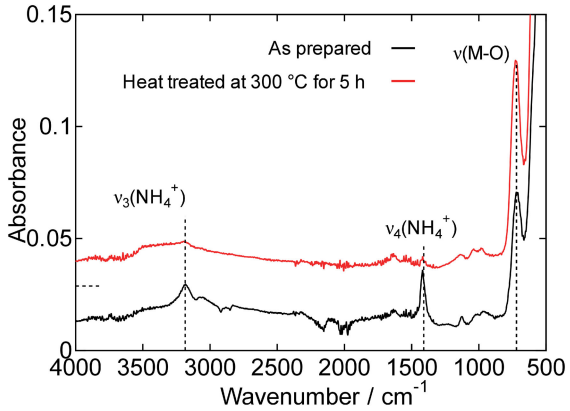

Fig. 3. ATR-FT-IR spectra of the samples prepared at $(x, y) = (0, 2)$ before and after heat treatment at 300 °C for 5 h in air.

subsequently kept stirring at 100 °C for t h. The suspensions did not boil probably because of their boiling point elevation.

Figure 2 shows powder XRD patterns of the samples prepared at $x = 0$ and $t = 2$, before heat treatment at 300 °C. Single-phase α-MnO_2[38] was obtained at $y = 2$, whereas ramsdellite-type R-MnO_2[39] were formed as an impurity phase at $y = 0$ and 1. Thus, $(NH_4)_2SO_4$ was necessary to synthesize single-phase α-MnO_2 in this process as an extra source of the template NH_4^+ ions and hereafter y was fixed at 2.

At $(x, y) = (0, 2)$, single-phase α-MnO_2 was obtained at $t = 0$, 1, and 2. The yield of these powder samples was calculated as the ratio of their mass after heat treatment at 300 °C for 5 h in air to the ideal mass of MnO_2 of 15 mmol. The yields at $t = 0$, 1, and 2 were ~0.63, ~0.93 and ~0.97, respectively. Thus, the reaction appears to be mostly completed at $t = 1$, whereas all samples in subsequent experiments were prepared at $t = 2$ to ensure the completion of the hydrothermal reaction.

Figure 3 shows the ATR-FT-IR spectra of the samples prepared at $(x, y) = (0, 2)$ before and after heat treatment at 300 °C. In the as-prepared sample, absorption bands attributed to the asymmetric stretching (ν_3) and bending (ν_4) modes of NH_4^+ ions, probably located in the channels of hollandite-type α-MnO_2, were observed at ~3200 and ~1450 cm^{-1}, respectively.[41] These absorption bands were almost absent after heat treatment at 300 °C, indicating that this heat treatment is effective for eliminating interstitial NH_4^+ ions.

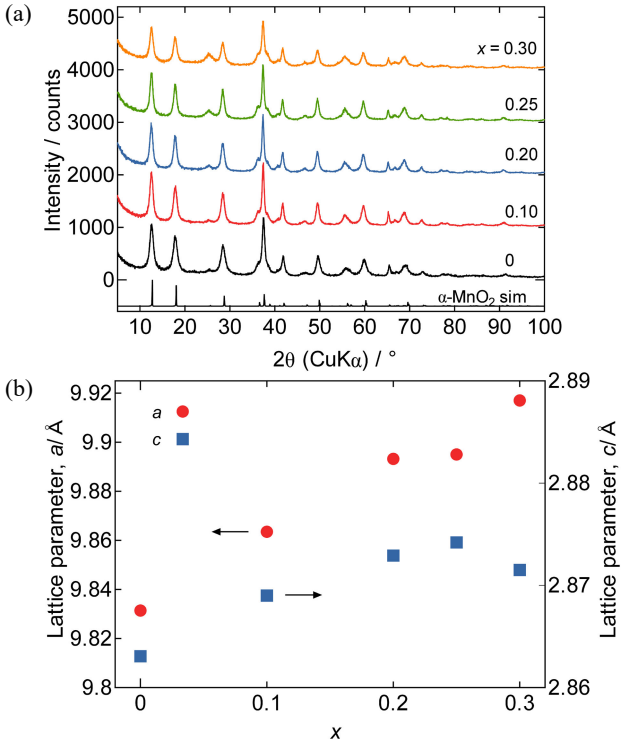

Fig. 4. (a) Powder XRD patterns of the samples prepared at $y = 2$ after heat treatment at 300 °C for 5 h in air, and simulated pattern of α-MnO_2 calculated using RIETAN-FP[40] and the structure parameters reported in Ref. 38). (b) Variation of lattice parameters with x.

Figure 4(a) shows powder XRD patterns of the samples after heat treatment at 300 °C for 5 h in air. The Rietveld refinements of these patterns shown in Fig. S1 indicated that hollandite-type single-phase samples were obtained at $x \leq 0.2$, whereas anatase-type TiO_2[42] was formed as a minor impurity phase at $x = 0.25$ and 0.30. The refined structure parameters are listed in Tables S1–S5. Refinements with small electron density (O3) in the channels gave better results, whereas the origin of the electron density remains uncertain. Figure 4(b) shows the dependence of lattice parameters on x of the hollandite phase derived by the Rietveld refinement. Lattice parameters a and c increased linearly with x at $x \leq 0.2$. This increase in unit cell dimensions is consistent with the larger ionic radius of a Ti^{4+} ion (0.75 Å[43]) than a Mn^{4+} ion (0.67 Å[43]) in an octahedral coordination. These observations confirmed the formation of the solid solution α-$Mn_{1-x}Ti_xO_2$. The solubility limit of Ti with this process was $x \simeq 0.2$.

Figure 5 shows the FE-SEM images of the samples. At $x = 0$, rod-shaped primary particles typical of hydrothermally synthesized α-MnO_2[11,21] were clearly seen. The incorporation of Ti reduced both the length and diameter

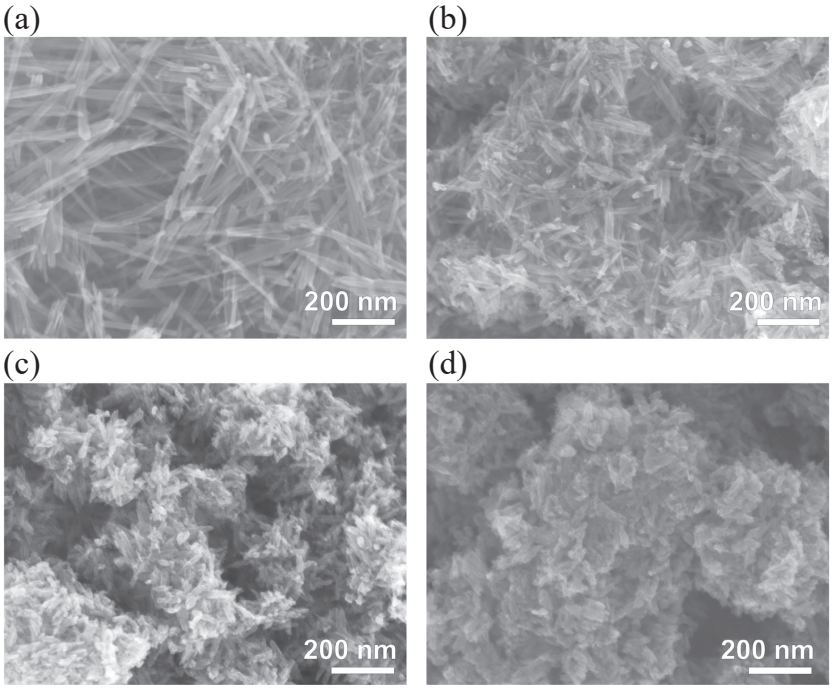

Fig. 5. FE-SEM images of the samples prepared at $y = 2$ and (a) $x = 0$, (b) 0.10, (c) 0.20, and (d) 0.25.

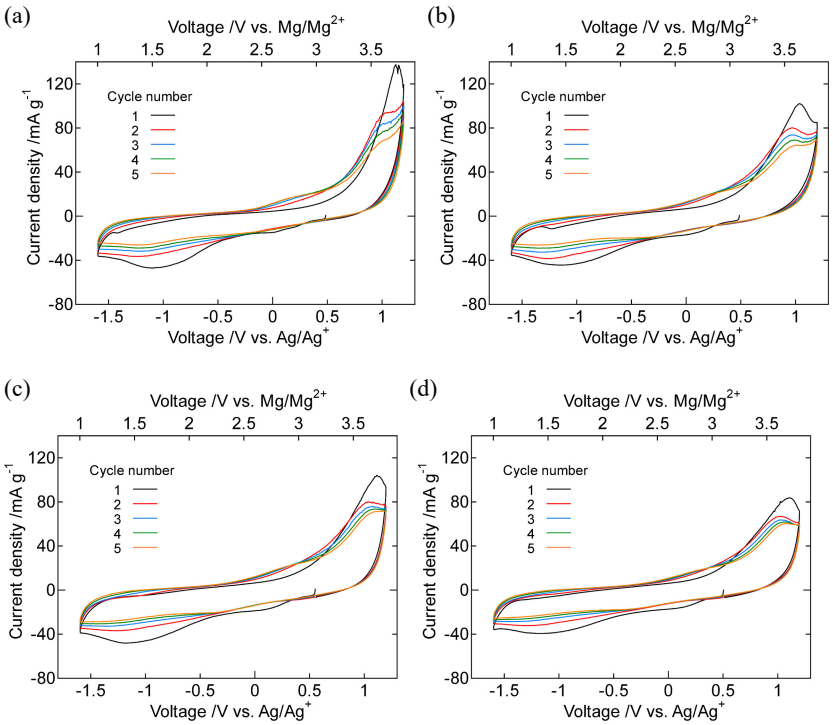

Fig. 6. Cyclic voltammograms of dry composite cathodes of the samples prepared at $y = 2$ and (a) $x = 0$, (b) 0.10, (c) 0.20, and (d) 0.25 in 0.3 mol dm^{-3} [Mg(G4)][TFSA]$_2$/[C$_3$mPyr][TFSA] at 80 °C.

of the primary particles. These results suggest the suppression of crystal growth with the addition of Ti. The BET specific surface areas of the samples prepared at $x = 0$, 0.10, 0.20, and 0.25 were ~130, ~166, ~183, and ~199 m^2 g^{-1}, respectively. This increase in specific surface area with x was consistent with the reduction of average primary particle size.

Figure 6 shows the cyclic voltammogram of the samples. The cathodic peak observed at ~1.5 V vs. Mg/Mg^{2+} was attributed to the insertion of Mg^{2+} ions in α-$Mn_{1-x}Ti_xO_2$ and the resulting reduction of Mn^{4+} and/or Mn^{3+} ions.[10] In contrast, the anodic peak at ~3.5 V vs. Mg/Mg^{2+} was due to the oxidation of Mn^{2+} and/or Mn^{3+} ions associated with the extraction of Mg^{2+} ions. The

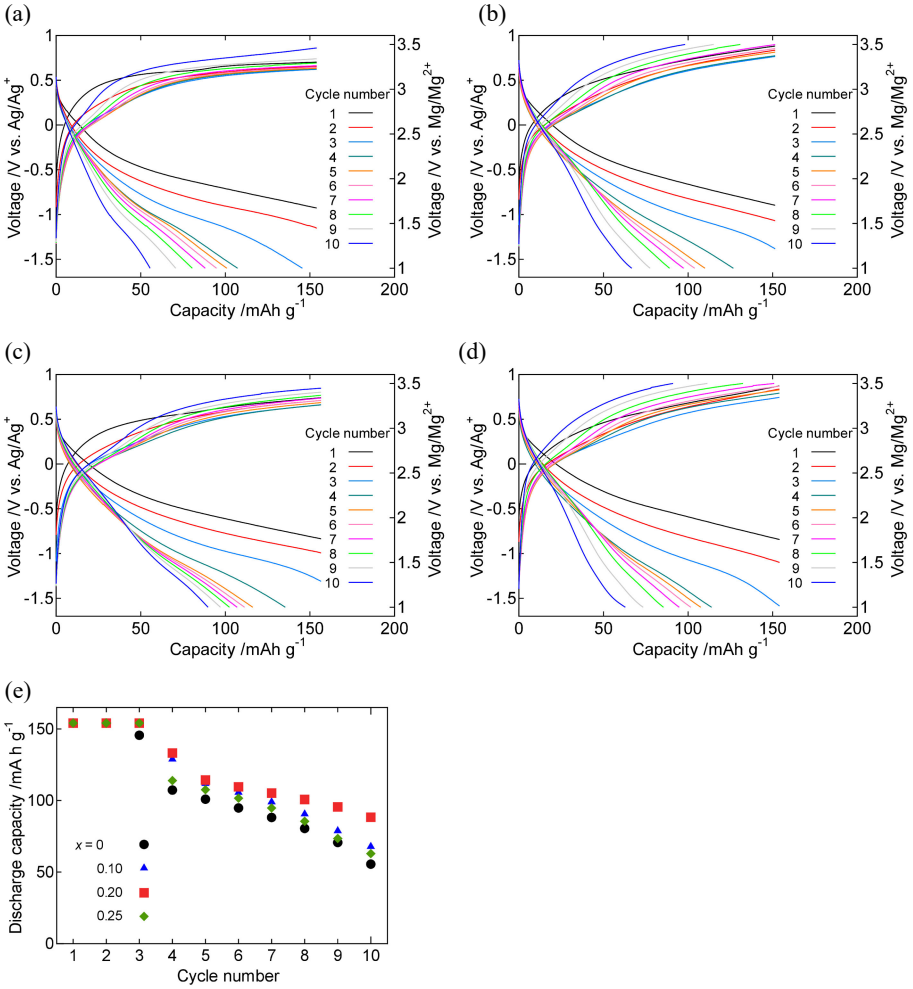

Fig. 7. Galvanostatic charge–discharge curves of dry composite cathodes of the samples prepared at $y = 2$ and (a) $x = 0$, (b) 0.10, (c) 0.20, and (d) 0.25 in 0.3 mol dm^{-3} [Mg(G4)][TFSA]$_2$/[C_3mPyr][TFSA] at 80 °C. (e) Discharge capacity retention of the samples shown in panels (a)–(d).

anodic current at $\gtrsim$ 3.6 V vs. Mg/Mg^{2+}, originated from oxidative electrolyte decomposition on sample surfaces, was the largest in the Ti-free ($x = 0$) sample. However, the anodic current was suppressed in the samples containing Ti ($x \geq 0.1$), despite an increase in surface area with x, indicating that the incorporation of Ti is effective in reducing catalytic activity for oxidative electrolyte decomposition on α-MnO_2.

Figure 7 shows the galvanostatic charge–discharge curves and capacity retention of dry composite cathodes of the samples in 0.3 mol dm^{-3} [Mg(G4)][TFSA]$_2$/[C_3mPyr][TFSA] at 80 °C. The sample prepared at $x = 0$ exhibited a plateau at ~3.2 V vs. Mg/Mg^{2+}, attributed to oxidative electrolyte decomposition. In contrast, such a plateau was absent, and charge voltage increased monotonically in the samples containing Ti. These observations are consistent with the cyclic voltammograms shown in Fig. 6. In all samples discharge capacity reached the capacity cutoff (154 mA h g^{-1}) in the 1st and 2nd discharge, whereas it decreased with cycle number after that. The discharge capacity at the 10th cycle was ~55 mA h g^{-1} in α-MnO_2 prepared at $x = 0$, whereas the sample prepared at $x = 0.20$ exhibited a better discharge capacity of ~85 mA h g^{-1} after the 10th cycle. The capacity retention of the sample prepared at $x = 0.25$ was worse than that of the sample prepared at $x = 0.20$, probably because of the formation of the secondary TiO_2 phase.

Figure 8 shows the galvanostatic charge–discharge curves and discharge capacity retention of dry composite cathodes of the samples in Mg[B(HFIP)$_4$]$_2$/G3 at 30 °C. In the 1st cycle, discharge capacity reached 154 mA h g^{-1} in all samples. The sample prepared at $x = 0$ maintained this discharge capacity up to the 3rd cycle, whereas the capacity fading in the subsequent cycles was faster than that of the samples containing Ti. In addition, the incorporation of Ti reduced the increment of charge overvoltage during cycles. Discharge capacity after the 10th cycle was better for the sample prepared at $x = 0.20$ (~75 mA h g^{-1}) than for the one prepared at $x = 0$ (~40 mA h g^{-1}). The partial cation substitution with Ti may stabilize the hollandite-type crystal structure, leading to an improvement of electrochemical properties.

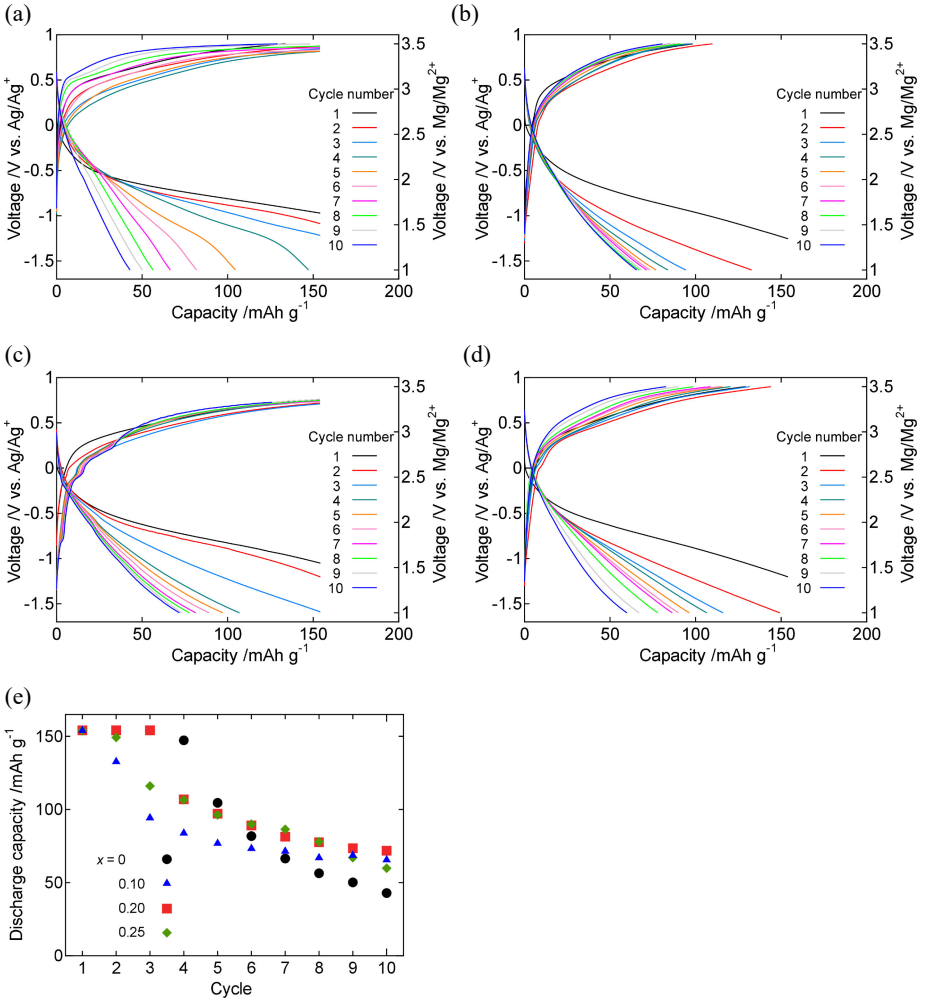

Fig. 8. Galvanostatic charge–discharge curves of dry composite cathodes of the samples prepared at $y = 2$ and (a) $x = 0$, (b) 0.10, (c) 0.20, and (d) 0.25 in 0.3 mol dm^{-3} $Mg[B(HFIP)_4]_2$/G3 at 30 °C. (e) Discharge capacity retention of the samples shown in panels (a)–(d).

4. Conclusions

A hydrothermal method to prepare hollandite-type α-MnO_2 under atmospheric pressure was developed and solid solutions α-$Mn_{1-x}Ti_xO_2$ were synthesized as new cathode materials for RMBs. The synthesis of α-$Mn_{1-x}Ti_xO_2$ was completed within 2 h and the solubility limit of Ti was $x \simeq 0.2$. The partial cation substitution of Ti in α-MnO_2 suppressed the growth of primary particles and increased surface area, whereas it depressed anodic current attributed to oxidative electrolyte decomposition during charging. The partial Ti substitution decreased overpotential during charging and improved the electrochemical properties. These observations indicated that α-$Mn_{1-x}Ti_xO_2$ with $x = 0.2$ is suitable for the cathode active materials of RMBs.

Acknowledgments This work was supported by GteX Program Japan Grant Number JPMJGX23S1. The authors thank Dr. Yuma Shimbori for assistance with electrochemical measurements.

References

1) S. Okamoto, T. Ichitsubo, T. Kawaguchi, Y. Kumagai, F. Oba, S. Yagi, K. Shimokawa, N. Goto, T. Doi and E. Matsubara, *Adv. Sci.* 2, 1500072 (2015).
2) J. Han, S. Yagi and T. Ichitsubo, *J. Power Sources* 435, 226822 (2019).
3) H. Kobayashi, K. Samukawa, M. Nakayama, T. Mandai and I. Honma, *ACS Appl. Nano Mater.* 4, 8328 (2021).
4) K. Shimokawa, T. Atsumi, N. L. Okamoto, T. Kawaguchi, S. Imashuku, K. Wagatsuma, M. Nakayama, K. Kanamura and T. Ichitsubo, *Adv. Mater.* 33, 2007539 (2021).
5) K. Sone, Y. Hayashi, T. Mandai, S. Yagi, Y. Oaki and H. Imai, *J. Mater. Chem. A* 9, 6851 (2021).
6) Y. Idemoto, M. Takamatsu, C. Ishibashi, N. Ishida, T. Mandai and N. Kitamura, *J. Electroanal. Chem.* 928, 117064 (2023).
7) R. Zhang, X. Yu, K.-W. Nam, C. Ling, T. S. Arthur, W. Song, A. M. Knapp, S. N. Ehrlich, X.-Q. Yang and M. Matsui, *Electrochem. Commun.* 23, 110 (2012).
8) T. S. Arthur, R. Zhang, C. Ling, P.-A. Glans, X. Fan, J. Guo and F. Mizuno, *ACS Appl. Mater. Inter.* 6, 7004 (2014).

9) J.-S. Kim, W.-S. Chang, R.-H. Kim, D.-Y. Kim, D.-W. Han, K.-H. Lee, S.-S. Lee and S.-G. Doo, *J. Power Sources* **273**, 210 (2015).
10) X. Ye, H. Li, T. Hatakeyama, H. Kobayashi, T. Mandai, N. L. Okamoto and T. Ichitsubo, *ACS Appl. Mater. Interfaces* **14**, 56685 (2022).
11) K. Shimokawa, T. Hatakeyama, H. Li and T. Ichitsubo, *Curr. Opin. Electrochem.* **38**, 101209 (2023).
12) T. Kawaguchi, N. Nemoto, H. Sakurai, N. L. Okamoto and T. Ichitsubo, *Chem. Mater.* **36**, 4877 (2024).
13) C. Ling, R. Zhang, T. S. Arthur and F. Mizuno, *Chem. Mater.* **27**, 5799 (2015).
14) T. Hatakeyama, H. Li, N. L. Okamoto, K. Shimokawa, T. Kawaguchi, H. Tanimura, S. Imashuku, M. Fichtner and T. Ichitsubo, *Chem. Mater.* **33**, 6983 (2021).
15) I. Oda-Bayliss, S. Yagi, M. Kamiko, K. Shimada, H. Kobayashi and T. Ichitsubo, *J. Mater. Chem. A* **12**, 17510 (2024).
16) Y. Qi, H. Li, K. Shimokawa, X. Ye, T. Kawaguchi and T. Ichitsubo, *J. Phys. Chem. C* **127**, 21271 (2023).
17) M. Latroche, L. Brohan, R. Marchand and M. Tournoux, *J. Solid State Chem.* **81**, 78 (1989).
18) T. Sasaki, M. Watanabe and Y. Fujiki, *Acta Crystallogr. B* **49**, 838 (1993).
19) Y. F. Shen, R. P. Zerger, R. N. DeGuzman, S. L. Suib, L. McCurdy, D. I. Potter and C. L. O'Young, *Science* **260**, 511 (1993).
20) R. Chen, P. Zavalij and M. S. Whittingham, *Chem. Mater.* **8**, 1275 (1996).
21) X. Wang and Y. Li, *J. Am. Chem. Soc.* **124**, 2880 (2002).
22) X. Wang and Y. Li, *Chem.-Eur. J.* **9**, 300 (2003).
23) L. Li, Y. Pan, L. Chen and G. Li, *J. Solid State Chem.* **180**, 2896 (2007).
24) G. Cao, L. Su, X. Zhang and H. Li, *Mater. Res. Bull.* **45**, 425 (2010).
25) J.-H. Moon, H. Munakata, K. Kajihara and K. Kanamura, *Electrochemistry* **81**, 2 (2013).
26) T. Hatakeyama, N. L. Okamoto and T. Ichitsubo, *J. Solid State Chem.* **305**, 122683 (2022).
27) R. Hypôlito, J. V. Valarelli, R. Giovanoli and S. M. Netto, *Chimia* **38**, 427 (1984).
28) T. Ohzuku, J. Kato, K. Sawai and T. Hirai, *J. Electrochem. Soc.* **138**, 2556 (1991).
29) R. N. DeGuzman, Y.-F. Shen, E. J. Neth, S. L. Suib, C.-L. O'Young, S. Levine and J. M. Newsam, *Chem. Mater.* **6**, 815 (1994).
30) R. Iimura, S. Kawasaki, T. Yabu, S. Tachibana, K. Yamaguchi, T. Mandai, K. Kisu, N. Kitamura, Z. Zhao-Karger, S. Orimo, Y. Idemoto, M. Matsui, M. Fichtner, I. Honma, T. Ichitsubo and H. Kobayashi, *Small* **21**, 2411493 (2025).
31) M. N. Babu, K. K. Sahu and B. D. Pandey, *Hydrometallurgy* **64**, 119 (2002).
32) K. M. Parida, S. B. Kanungo and B. R. Sant, *Electrochim. Acta* **26**, 435 (1981).
33) S. Terada, T. Mandai, S. Suzuki, S. Tsuzuki, K. Watanabe, Y. Kamei, K. Ueno, K. Dokko and M. Watanabe, *J. Phys. Chem. C* **120**, 1353 (2016).
34) T. Mandai, K. Tatesaka, K. Soh, H. Masu, A. Choudhary, Y. Tateyama, R. Ise, H. Imai, T. Takeguchi and K. Kanamura, *Phys. Chem. Chem. Phys.* **21**, 12100 (2019).
35) Z. Zhang, Z. Cui, L. Qiao, J. Guan, H. Xu, X. Wang, P. Hu, H. Du, S. Li, X. Zhou, S. Dong, Z. Liu, G. Cui and L. Chen, *Adv. Energy Mater.* **7**, 1602055 (2017).
36) Z. Zhao-Karger, M. E. Gil Bardaji, O. Fuhr and M. Fichtner, *J. Mater. Chem. A* **5**, 10815 (2017).
37) T. Mandai, *ACS Appl. Mater. Interfaces* **12**, 39135 (2020).
38) Y. D. Kondrashev and A. I. Zaslavskii, *Izv. Akad. Nauk SSSR Ser. Fiz.* **15**, 179 (1951).
39) C. Fong, B. J. Kennedy and M. M. Elcombe, *Z. Kristallogr.* **209**, 941 (1994).
40) F. Izumi and K. Momma, *Solid State Phenom.* **130**, 15 (2007).
41) H. B. Wu, M. N. Chan and C. K. Chan, *Aerosol Sci. Technol.* **41**, 581 (2007).
42) M. Horn, C. F. Schwebdtfeger and E. P. Meagher, *Z. Kristallogr.* **136**, 273 (1972).
43) R. D. Shannon, *Acta Crystallogr.* **32**, 751 (1976).